



HAL
open science

Fe-MOGs-based enzyme mimetic and its mediated electrochemiluminescence for in situ detection of H₂O₂ released from Hela cells

Li-Ping Zong, Ling-Yu Ruan, Junji Li, Robert S Marks, Jun-Song Wang, Serge Cosnier, Xue-Ji Zhang, Dan Shan

► To cite this version:

Li-Ping Zong, Ling-Yu Ruan, Junji Li, Robert S Marks, Jun-Song Wang, et al.. Fe-MOGs-based enzyme mimetic and its mediated electrochemiluminescence for in situ detection of H₂O₂ released from Hela cells. *Biosensors and Bioelectronics*, 2021, 184, pp.113216. <10.1016/j.bios.2021.113216>. <hal-03382950>

HAL Id: hal-03382950

<https://hal.science/hal-03382950v1>

Submitted on 18 Oct 2021

HAL is a multi-disciplinary open access archive for the deposit and dissemination of scientific research documents, whether they are published or not. The documents may come from teaching and research institutions in France or abroad, or from public or private research centers.

L'archive ouverte pluridisciplinaire **HAL**, est destinée au dépôt et à la diffusion de documents scientifiques de niveau recherche, publiés ou non, émanant des établissements d'enseignement et de recherche français ou étrangers, des laboratoires publics ou privés.



HAL Authorization

Fe-MOGs-based Enzyme Mimetic and Its Mediated Electrochemiluminescence for in situ Detection of H₂O₂ Released from HeLa Cells

Li-Ping Zong[†], Ling-Yu Ruan[†], Junji Li^{†}, Robert S. Marks[‡], Jun-Song Wang[†], Serge Cosnier[§], Xue-Ji Zhang[†], Dan Shan^{†*}*

[†] School of Environmental and Biological Engineering, Nanjing University of Science and Technology, Nanjing 210094, China

[‡] Department of Biotechnology Engineering, Ben-Gurion University of the Negev, Beer-Sheva, Israel.

[§] University of Grenoble Alpes-CNRS, DCM UMR 5250, F-38000 Grenoble, France

* Corresponding author:

Email: danshan@njust.edu.cn (D. Shan)

junjili@njust.edu.cn (J. Li)

Fax: 0086-25-84303107

ABSTRACT

Enzyme mimetics have attracted wide interest due to their inherent enzyme-like activity and unique physicochemical properties, as well as promising applications in disease diagnosis, treatment and monitoring. Inspired by the attributes of nonheme iron enzymes, synthetic models were designed to mimic their capability and investigate the catalytic mechanisms. Herein, metal-organic gels (Fe-MOGs) with horseradish peroxidase (HRP) like Fe-N_x structure were successfully synthesized through the coordination between iron and 1,10-phenanthroline-2,9-dicarboxylic acid (PDA) and exhibited excellent peroxidase-like activity. Its structure-activity relationship and the *in-situ* electrochemiluminescence (ECL) detection of H₂O₂ secreted by Hela cells were further investigated. The highly dispersed Fe-N_x active sites inside Fe-MOGs were able to catalyze the decomposition of H₂O₂ into large amounts of reactive oxygen species (ROS) *via* a Fenton-like reaction under a low overpotential. Due to the accumulation of ROS free radicals, the luminol ECL emission was significantly amplified. A proof-of-concept biosensor was constructed with a detection limit as low as 2.2 nM and a wide linear range from 0.01 to 40 μM. As a novel metal organic gels based enzyme mimetic, Fe-MOGs show great promises in early cancer detection and pathological process monitoring.

KEYWORDS: 1,10-phenanthroline-2,9-dicarboxylic acid (PDA), enzyme mimetic, electrochemiluminescence (ECL), hydrogen peroxide, Hela cells

1. Introduction

Natural enzymes are exquisite biocatalysts that mediate every life process in an organism and are widely applied in various fields due to remarkable catalytic efficiency and substrate specificity (Harrigan et al. 2018; Piazza et al. 2018; Zhang 2017). But due to their inherent defects hindering the practical application of enzymes, such as low operational stability, high cost of preparation and purification, developing enzyme substitutes has remained an outstanding challenge.

Enzyme mimetics, nanomaterials with enzyme-like characteristics, have attracted broad interest into their application and mechanisms of action (Wei and Wang 2013). The reactivity of enzyme mimetics bears clear resemblance to that of natural enzymes, and show advantages such as low cost, high stability and commercial accessibility (Wu et al. 2019). Several approaches have been undertaken to attain high reactivity of enzyme mimetics, such as controlling the size, morphology, and composition, forming hybrids, using external stimuli, etc. (Bete et al. 2019; Chen et al. 2018; Ding et al. 2019; Hu et al. 2017; Klunker et al. 2017; Liu et al. 2019; Singh et al. 2017; Sun et al. 2013). With the in-depth study of the physicochemical properties and catalytic mechanism of natural enzymes, simulating the structure of active center of enzyme can be a promising method (Bete et al. 2019; Wang et al. 2019a).

Similar to metal organic frameworks (MOFs), metal organic gels (MOGs) are one kind of supramolecular assemblies driven by metal-ligand interactions. MOGs feature tunable-soft porosity, open metal sites for catalysis and rapid mass transfer or permeability, rendering convenience in imitating the active center of natural enzymes.

MOGs can be synthesized under mild conditions (e.g., room temperature, atmospheric pressure, neutral condition, short reaction time, routine solvent, etc.). Jiao et al. used potassium chloride (KCl) as template, dimethylimidazole (MI) as ligand to obtain enzyme mimetic. Compared with other metals Zn, Co, less electron transfer was observed between Fe atom and the adsorbed hydroxyl group, which is beneficial to reduce the energy barrier for the formation of hydroxyl radicals, thereby improving peroxidase-like activity (Jiao et al. 2020). The active center of horseradish peroxidase (HRP) is the axial coordination of heme iron with a histidine residue at the N-terminus. Herein, we took HRP as the simulation object. To mimic the planar Fe-N structure of HRP, 1,10-phenanthroline-2,9-dicarboxylic acid (PDA) was chosen as ligand to coordinate with iron. As an organic ligand rich in aromatic nitrogen heterocycles, PDA is hallmarked by general chelating and bridging capabilities and a large conjugated aromatic plane resulting from a synergistic combination of donor groups with multi-chelating sites (Miao et al. 2015; Mirzaei et al. 2019). These properties contribute to construct metal clusters with high preorganization and thermodynamic stability.

In this work, a kind of two-dimensional sheet-like Fe-MOGs were synthesized by a one-step rapid reaction at room temperature. Structural information and electrochemical performance were systematically evaluated to reveal structure-activity relationship of the enzyme mimetic. The resultant Fe-MOGs possessed Fe-N_x catalytic sites similar to HRP, and exhibited exceptional activity for the decomposition of H₂O₂. A Fe-MOGs based luminol-H₂O₂ ECL platform was further applied for *in-situ* detection of H₂O₂ generated from Hela cells. The excellent performance of the proposed method

indicated promising application of MOGs in the medical detection and monitoring of biological small molecules.

2. Experimental section

2.1 Materials and Reagents

All reagents were commercially available and used without further pretreatments or purifications. 1,10-phenanthroline-2,9-dicarboxylic acid (PDA) and luminol were purchased from Aladdin Biochemical Technology Co., Ltd. (Shanghai, China). Iron(II) acetate ($\text{Fe}(\text{OAc})_2$) was obtained from Strem Chemicals, Inc. (Newburyport, USA). Dimethyl sulfoxide (DMSO), H_2O_2 and chitosan (low viscosity: < 200 mPa. s) were supplied by Sinopharm Chemical Reagent Co. Ltd. (Beijing, China). HeLa cells were obtained from National Infrastructure of Cell Line Resource (Beijing, China). Dulbecco's modified Eagle's medium (DMEM, 10%) was purchased from Gibco Laboratories Life Technologies Inc. (Grand Island, NY). Fetal bovine serum (FBS) was purchased from Gemini Bio Co., Ltd. (California, US). Lipopolysaccharide (LPS) and 3, 5, 3', 5'-tetramethylbenzidine (TMB) were purchased from Beyotime Biotechnology Inc. (Shanghai, China). Horseradish peroxidase (HRP) was purchased from Solarbio Science & Technology Co., Ltd. (Beijing, China). Luminol (3-aminophthalhydrazide) stock solution (0.01 M) was prepared in a 0.1 M NaOH solution and stored in a 4 °C refrigerator for at least 2 weeks before use. All aqueous solutions were prepared with deionized water obtained from a Millipore water purification system (≥ 18 M Ω , Milli-Q, Millipore).

2.2 Apparatus

Ultraviolet-vis (UV-Vis) spectra were recorded on the Shimadzu UV-3600 spectrophotometer. Fourier-transformation infrared (FT-IR) spectra were obtained with an IR-Prestige-21 FT-IR spectrometer (Shimadzu Co., Japan). Photoluminescence (PL) spectra were recorded by an Edinburgh FLS920 fluorescence spectrometer (Livingston, UK). The morphology was investigated with a XL-30E scanning electron microscope (SEM) and a Tecnai G2 20 LaB₆ high resolution transmission electron microscopy (HRTEM, FEI Co., USA). The X-ray photoelectron spectroscopy (XPS) experiments were carried out on K-Alpha (Thermo Fisher Scientific Co., USA). Cyclic voltammetry (CV) measurements were carried out on a CHI 660D electrochemical workstation (Chenhua, China) at room temperature. ECL studies were performed on an MPI-EII multifunctional electrochemical and chemiluminescent analytical system (Xi'an Remex Analytical Instrument Co., Ltd, China), and the photomultiplier tube was set at 1000 V, the magnification level was 3. An Autolab PGSTAT30 (Eco Chemie) which was controlled by NOVA 1.10 software was applied for Electrochemical impedance spectroscopy (EIS) measurement. All electrochemical studies were performed with a conventional three-electrode system, a bare or modified glassy carbon electrode (GCE, 5 mm in diameter) as working electrode, a saturated calomel electrode as reference electrode and a Pt wire as counter electrode.

2.3 Methods

Synthesis of the Fe-MOGs

The detailed preparation process of Fe-MOGs was according to the literature with a slight modification (He et al. 2017). In a typical one-step synthesis, 10 mM Fe(OAc)₂

(10.0 mL) aqueous solution was added dropwise into the DMSO solution of 10 mM PDA (10.0 mL). The above mixed light yellow solution was stirred vigorously for 30 s at room temperature. The light yellow powder denoted as Fe-MOGs was then collected by centrifugation (8000 rpm), washed with ethanol three times and freeze-dried overnight in a vacuum.

Peroxidase activity assay of the Fe-MOGs

The GCE was respectively polished with 0.3 and 0.05 μm alumina powder and rinsed by deionized water for further use. For the cyclic voltammetry test, 10 μL of the Fe-MOGs solution (2 mg mL^{-1}) and 10 μL of HRP in 0.01 M, pH 7.4 PBS solution (2 mg mL^{-1}) was dripped on the surface of GCE and dried at $37\text{ }^\circ\text{C}$ to obtain Fe-MOGs/GCE and HRP/GCE, respectively.

Hela cells culture and in vitro cytotoxicity

Hela cells were grown in Dulbecco's modified Eagle's medium (DMEM, 10%) containing FBS (10%), L-glutamine (4 mM), penicillin (100 units mL^{-1}), and streptomycin (100 mg mL^{-1}) under oxidative stress conditions ($1\text{ }\mu\text{g mL}^{-1}$ lipopolysaccharide (LPS)), and then incubated in a humidified atmosphere of 5% CO_2 at $37\text{ }^\circ\text{C}$. Hela cells were collected and suspended into sterilized PBS solution (0.01 M, pH 7.4) with specific concentration (cells mL^{-1}).

To investigate in vitro cytotoxicity of the Fe-MOGs, CCK-8 assay for Hela cells was performed. 100 μL of cells, at a density of 2×10^4 cells/well, were seeded into a 96-well plate, and incubated for 24 h at $37\text{ }^\circ\text{C}$ in a humidified 5% CO_2 -containing atmosphere. Then various concentrations of mixed Fe-MOGs/luminol were added. The

cells were incubated for an additional 24 h at 37 °C. 10 μL of CCK-8 solution was then added and incubated for 0.5 h. Untreated cells were used as controls. The absorbance was measured at a wavelength of 450 nm.

***In situ* detection for H_2O_2 released from HeLa cells**

For ECL detection of H_2O_2 , 15 μL 2 mg mL^{-1} Fe-MOGs aqueous solution and 15 μL 0.01 M luminol in 0.1 M NaOH aqueous solution were pre-mixed prior to modifying the GCE and then dried at 37 °C to obtain Fe-MOGs/luminol/GCE. Different concentrations of H_2O_2 were added into 4 mL of PBS working buffer. For ECL detection of HeLa cells, different amounts of HeLa cells and chitosan aqueous solution (0.1% wt) were pre-mixed and dripped on the Fe-MOGs/luminol/GCE to obtain HeLa cells/chitosan/Fe-MOGs/luminol/GCE. HeLa cells were adhered on the surface of Fe-MOGs/luminol/GCE by chitosan aqueous solution. ECL detection was studied at a scan rate of 30 mV s^{-1} within the scan range from 0 to 0.8 V.

3. Results and discussions

3.1 Synthesis and characterization of the Fe-MOGs

The procedures for the enzyme mimetic synthesis and the ECL immunosensor fabrication were illustrated in Scheme 1. In order to obtain the Fe- N_x structure containing HRP-like enzyme mimetic, $\text{Fe}(\text{OAc})_2$ and PDA were selected as the metal precursor and source of nitrogen. PDA can effectively chelate iron ions to achieve gel in a short time owing to the possible interactions between oxygen-containing groups, nitrogen-containing groups and metallic irons.

[Scheme 1]

In order to verify the synthesis a success or not, spectral data of the as-prepared sample were collected first. The UV-vis absorption spectra (Figure 1A) of the Fe-MOGs (curve c) shows an absorption at 230 nm standing for K-E combined band, which is caused by the conjugation effect of carboxyl group to benzene ring and an absorption at 254 nm standing for B band (Xu et al. 2019), demonstrating the existence of PDA in the prepared samples. A certain blue shift of Fe-MOGs/luminol (curve d) occurred in the absorption peaks at 290 nm compared with luminol (curve e) due to the interaction with the Fe-MOGs. Therefore, luminol was demonstrated to be successfully functionalized with the Fe-MOGs.

In FTIR spectra (Figure 1B), the C=N skeleton vibration of Fe-MOGs (1467 cm^{-1}) (curve a) is blue-shifted relative to the C=N skeleton vibration of PDA (1448 cm^{-1}) (curve b) (Mirzaei et al. 2019), which is most likely due to the increased electronegativity of pyridine N in PDA after donating a lone electron pair to iron ion, resulting in an enhanced polarity of the chemical bond between N and C on the pyridine ring. Also the attenuation of $\nu(\text{C}=\text{O})$ absorption around 1719 cm^{-1} in the Fe-MOGs can be ascribed to deprotonation of carboxyl groups in the ligands, implying the complete deprotonation of the carboxylic groups in the PDA^{2-} ligands (Mirzaei et al. 2019; Ramezanpour et al. 2019). Fluorescent spectroscopic measurements were also conducted for more detailed structural information. As depicted in Figure 1C, the Fe-MOGs (curve a) shows little fluorescent emission in comparison with PDA (curve b),

which might be assigned to the decrease in the density of π electron clouds on the ring offset around the nitrogen atom due to the formation of Fe-N bonds even though the lone electron pair of N does not participate in conjugation.

The morphological data were characterized by scanning electron microscopy (SEM) and transmission electron microscope (TEM). As shown in Figure 1D, 1E and 1F, the observed morphology of the Fe-MOGs distributed in thin layer sheet form, which may be beneficial for the mass transfer of Fe-N_x active sites HRP. The surface compositions and electronic states were further investigated by X-ray photo-electron spectroscopy (XPS), confirming the presence of C, N, O and Fe (Figure S1). As shown in Figure 1G, the Fe 2p_{1/2} and 2p_{3/2} regions are fitted with Fe(II), Fe(III) and their respective satellite peaks. The two main peaks in the Fe 2p_{3/2} region have positions of 709.9 and 711.7 eV and can be assigned to Fe²⁺ and Fe³⁺ oxidation state respectively (Sun et al. 2019). These results indicate that iron on the Fe-MOGs is mainly in the Fe²⁺ state, which is consistent with the light yellow colour of samples. The high-resolution N 1s spectrum of the Fe-MOGs displays three deconvoluted peaks ascribed to Fe-N_x (399.5 eV), and pyridinic N (398.6 eV) as well as π - π^* satellite (406.1 eV) (Figure 1H) (Hou et al. 2020; Jiao et al. 2020; Lou et al. 2020), further demonstrating the formation of Fe-N_x active sites. Fitted high-resolution C 1s spectrum evidences the presence of indefinite C-C (284.8 eV), C-N (285.7 eV), O-C=O (288.2 eV) (Figure 1I) (Hou et al. 2020). Thus, on the basis of the preceding surveys, it is rational to come to the conclusion that the coordination between iron ions, bidentate nitrogen heterocycles can endow the Fe-MOGs a structure similar to the active center of natural HRP.

[Figure 1]

3.2 Electrochemical performance of the Fe-MOGs

Due to the similar Fe-N_x active sites to the natural HRP, the Fe-MOGs with Fe-N_x active sites are expected to possess the intrinsic peroxidase activity. It is well known that the active center of peroxidase such as HRP is located at the metal-N site. Considering the presence of Fe-N sites in the structure, we suspected that the Fe-MOGs may have catalytic properties similar to those of peroxidase. The HRP-like activity of Fe-MOGs was confirmed *via* the reaction of 3, 5, 3', 5'-tetramethylbenzidine (TMB), and the absorbance band at 652 nm, originating from the oxidation product of TMB, is observed in the presence of Fe-MOGs and H₂O₂ (Figure S2A). Furthermore, the absorbance at 652 nm increases with the increasing concentration of Fe-MOGs (Figure S2B). Electrochemical behaviors of the Fe-MOGs were investigated by cyclic voltammetry at 25°C in nitrogen saturated PBS solution (0.01 M, pH 7.4). As shown in Figure 2A, the electrochemical response of the Fe-MOGs (curve e) exhibited a redox peak attributed to the redox reaction of Fe(II)/Fe(III). Electric potential of anode peak and cathodic peak (E_{pa} , E_{pc}) are -0.053 V, -0.176 V at the scan rate of 10 mV s⁻¹, respectively. The anode peak and cathodic peak currents (I_{pa} , I_{pc}) vary linearly with the square root of scan rate (Figure S3), indicating characteristic behavior of diffusion controlled redox species. The linear regression equation is I_{pa} (μA) = 0.35v^{1/2} + 3.05, R² = 0.9344; I_{pc} (μA) = -0.26v^{1/2} -1.52, R² = 0.9969, respectively. Electrocatalytic

properties of the Fe-MOGs were characterized by the comparative CV curves of Fe-MOGs/GCE in 0.01 M PBS solution containing different concentration of H₂O₂ (Figure 2B). The reduction peak current increases with the increase of H₂O₂ concentration, which is consistent with that of HRP (Figure S4), reflecting the HRP-like decomposition activity of Fe-MOGs on H₂O₂. And it can be implied that the catalytically active site Fe-N_x may participate in the electron transfer reaction by changing the valence state of the center iron ions. Figure S5A shows the current-time recordings of Fe-MOGs modified GCE to the successive addition of H₂O₂ at the potential of -0.3 V in 0.01 M, pH 7.4 PBS at room temperature. In addition, Michaelis-Menten kinetics of Fe-MOGs were investigated. The values obtained for the Michaelis-Menten constant (K_m) and maximum initial velocity (V_{max}) from the Lineweaver-Burk plot (Figure S5B inset) are 217.9 μM and 2.818 μM s⁻¹, respectively. The K_m value is much lower than that of HRP, 437.6 μM (Jiang et al. 2018a), indicating that a lower concentration of H₂O₂ was needed to reach the maximal catalytic activity of Fe-MOGs.

[Figure 2]

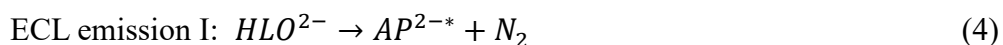
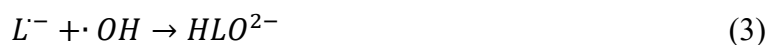
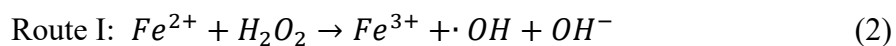
3.3 Mechanism research of ECL signal amplification

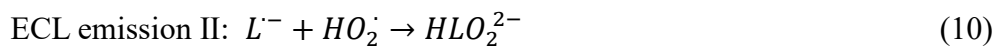
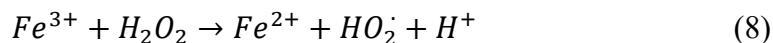
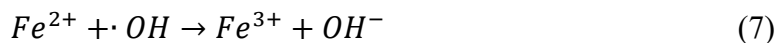
In the light of the mimic peroxidase activity of the Fe-MOGs, it is highly possible to mediate enhanced ECL emission in the luminol-H₂O₂ system. To study the role of Fe-MOGs in the luminol-H₂O₂ system, the ECL behaviors of Fe-MOGs/luminol/GCE and

luminol/GCE were investigated in 4.0 mL of PBS solution (0.01 M, pH 7.4) containing 15 μ M H₂O₂ respectively. It is shown in Figure 3A that the Fe-MOGs/GCE (curve d) showed no ECL performance confirming luminol the only luminophore and Fe-MOGs/luminol/GCE (curve a) and luminol/GCE (curve b) both had a cathode ECL emission at about 0.5 V attributed to luminol. The ECL intensity in the presence of the Fe-MOGs reached around 7000 a.u., about two times the intensity in the absence of the Fe-MOGs, which achieved approximately 3000 a.u., while PDA had negligible influence on the ECL intensity (curve c). And in the inset of Figure 3B, the decrease in the initial oxidation potential of Fe-MOGs/luminol (curve a) also illustrates that the Fe-MOGs can effectively enhance the ECL signal of luminol. On the other hand, in consideration of the redox potential of Fe(II)/Fe(III), the initial potential was optimized to improve accuracy of ECL detection. As shown in Figure S6A, in the absence of H₂O₂, the ECL of luminol/GCE under air (curve a) saturated atmosphere boosted compared with nitrogen saturated condition when the initial potential reached -0.4 V, which is the reduction potential of dissolved oxygen. While in the presence of 15 μ M H₂O₂ in Figure S6B, the ECL of Fe-MOGs/luminol/GCE increased simultaneously under air (curve a) and nitrogen (curve b) saturated atmosphere as the initial potential decreased, implying that the Fe-MOGs are not sensitive to dissolved oxygen and H₂O₂ is the only available co-reactant source in Fe-MOGs/luminol-H₂O₂ system. In this case, 0 V was selected as initial potential to achieve a strong ECL intensity in a comparatively narrow potential scanning window.

In order to reveal the mechanism of ECL signal amplification, comparative cyclic

voltammetry of Fe-MOGs/luminol modified GCE in 0.01 M, pH 7.4 PBS solution in the (a) absence and (b) presence of 15 μM H_2O_2 was conducted (Figure S7). An oxidization peak at about 0.49 V can be observed in both curves while stronger in the presence of 15 μM H_2O_2 . It corresponds to the oxidation of luminol which can be ascribed to the reduction of H_2O_2 (Wang et al. 2019b). To further clarify the proposed mechanism, the active intermediates formed in the ECL system were determined. As shown in Figure S8, the effects of different reactive oxygen species (ROS) scavengers on the ECL signal of Fe-MOGs/luminol- H_2O_2 and luminol- H_2O_2 system were studied. Isopropanol (IPA), benzoquinone (BQ) and L-Cysteine (L-Cys) were used to scavenge $\cdot\text{OH}$, $\text{O}_2\cdot^-$ and almost all ROS, respectively. The ECL intensity was obviously inhibited when 1.0 mM IPA and BQ was added to the electrolyte respectively and the ECL intensity was almost completely suppressed when 1.0 mM L-Cys was added, insinuating ROS like $\cdot\text{OH}$ and $\text{HO}_2\cdot^-$ might be produced in the system. And in the presence of Fe-MOGs, IPA achieved stronger quenching effect, indicating more $\cdot\text{OH}$ was generated in Fe-MOGs/luminol- H_2O_2 system. On this basis, a possible mechanism for luminol- H_2O_2 ECL systems based on Fe- N_x catalysts is described as follows.





First, luminol anions (LH^{-}) are electrochemically oxidized to luminol anionic radicals ($L^{\cdot-}$). In Route I [Eq. (2)], H_2O_2 is reduced by the FeN_X active sites to produce $\cdot OH$, and it is the decisive step. In Route II [Eq. (6)], followed by the oxidization of Fe^{2+} upon anodic potential scanning, H_2O_2 is catalyzed by the pre-oxidized FeN_X active sites to generate $HO_2\cdot$. Finally, rapidly accumulated ROS react with $L^{\cdot-}$ to form excited-state 3-aminophthalate anion (AP^{2-*}), thus achieving enhanced ECL emission.

3.4 Biosensor for *in situ* detection of H_2O_2 released from HeLa cells

H_2O_2 mediated inhibition of protein phosphatases contributes to oncogene overexpression, a hallmark of many cancers (Fruehauf and Meyskens 2007). The excessive levels of H_2O_2 cause oxidative damage to cellular protein, nucleic acids, and lipid molecules, thereby contributing to aging and age-related diseases including cancer. H_2O_2 content at the cellular level diversifies slightly from cancer cell to normal cell. The number of extracellular released H_2O_2 molecules is around 10^{11} per cell (Guo et al. 2010). Therefore, developing highly sensitive biosensor for trace detection of H_2O_2 at the cell level is of great reference significance for early cancer screening and population mixed sample detection. Relationship between ECL intensity and H_2O_2 concentrations was

determined in the next step for further fabrication of HeLa cell biosensor. The material capacity of electrode and the luminol concentration have been optimized. A capacity of $0.15 \mu\text{g cm}^{-2}$ Fe-MOGs demonstrates the best ECL performance and the optimized luminol concentration turns out to be 5 mM (Figure S9). As illustrated in Figure 3C, the ECL peak intensity is proportional to the concentration of H_2O_2 (0.01, 0.05, 0.1, 0.5, 1, 5, 10, 15, 20, 25, 30, 35, 40 μM), and two good linear segments were observed. As shown in Figure 3D and 3E, $I \text{ (a.u.)} = 188.89 + 788.77C \text{ (0.01-1 } \mu\text{M)}$, $R^2 = 0.993$ and $I \text{ (a.u.)} = 784.70 + 415.32C \text{ (1-40 } \mu\text{M)}$, $R^2 = 0.998$, respectively. The limit of detection (LOD) was calculated to be 2.2 nM (signal-to-noise ratio of 3). As shown in Table 1, compared with most of the reported electrochemical (EC), fluorescent (FL) and ECL sensors for H_2O_2 detection, our proposed ECL sensor displays high sensitivity with a low LOD of 2.2 nM. But further work is still necessitated to improve the sensitivity and simplify the fabrication of the sensor.

Furthermore, ECL potential cycling stability and long-term stability of the as-prepared sensor were tested. The ECL response of Fe-MOGs/luminol/GCE is observed with relative standard deviations (RSD) of 0.172% when tested in 0.01 M, pH 7.4 PBS containing 10 μM H_2O_2 upon 20 cycles of continuous cyclic scans between 0 ~ +0.8 V (Figure S10A), indicating the excellent ECL potential cycling stability for H_2O_2 assay. As shown in Figure S10B, the ECL response of Fe-MOGs/luminol/GCE in 0.01 M, pH 7.4 PBS containing 15 μM H_2O_2 was detected at one-day intervals for 9 days, which only slightly decreases after five tests with RSD 3.8%, reflecting a good long-term stability of this sensor. Selectivity was also investigated in Figure S11, compared with

10 μM H_2O_2 , the introduction of 1 mM Na^+ , Cl^- , NO_2^- , ascorbic acid (AA), glutamine (Gln) and glucose (Glu) had a negligible effect on the ECL signal. The ECL responses upon Ca^{2+} was obviously fluctuated, which may be affected by the chelation of the metal with the ligand. Overall, the survey results indicate that the prepared ECL sensor has a considerate stability and selectivity for H_2O_2 .

To study general applicability of the proposed sensor in real biological samples, ECL platform based on Fe-MOGs/luminol was exploited to evaluate the H_2O_2 generated from HeLa cells. To investigate the biocompatibility of the biosensor based on the Fe-MOGs, CCK-8 assay of HeLa cells that incubated with various concentrations of mixed Fe-MOGs/luminol was conducted. The initial concentrations of Fe-MOGs and luminol in the medium are 2 mg mL^{-2} and 10 mM, respectively. The concentration of the mixed Fe-MOGs/luminol was diluted 10, 40, 160, 640 and 2560 times, respectively. As shown in Figure S12A, Fe-MOGs/luminol displayed relatively low cytotoxicity for HeLa cells, as the viability remained above 69% after 24 h incubation time (Shamsipur et al. 2018). HeLa cells dispersed in 0.01 M, pH 7.4 PBS were prepared in advance. Since chitosan film is not only favorable for cell immobilization but also increases the space between cells and the electrode (Liu et al. 2018), chitosan (low viscosity: < 200 mPa. s) 0.1% wt aqueous solution was used as an intermediate binder for cell adhesion to the surface of the Fe-MOGs/luminol modified GCE. As shown in Figure S12B, the ECL response of Fe-MOGs/luminol/GCE modified with HeLa cells coated with chitosan is approximately three times that of Fe-MOGs/luminol/GCE modified with HeLa cells without chitosan. And the cell-free Fe-MOGs/luminol/GCE modified by chitosan has

almost no ECL response, indicating that chitosan facilitates cell immobilization without interfering with ECL detection. EIS was applied for characterizing the successful immobilization of HeLa cells onto the Fe-MOGs/luminol/GCE. The Nyquist plot of the Fe-MOGs/luminol and the chitosan-coated HeLa cells modified Fe-MOGs/luminol were displayed in Figure S12C. Compared with the semicircular diameter obtained from Fe-MOGs/luminol (curve a), the semicircular diameter of chitosan-coated HeLa cells modified Fe-MOGs/luminol is significantly increased (curve b), indicating the successful immobilization of chitosan-coated HeLa cells onto Fe-MOGs/luminol. In addition, similar to the literature, LPS was used to stimulate the production of H_2O_2 in cells (Jiang et al. 2018b). Control experiments were conducted to confirm the selectivity to H_2O_2 in this practical situation. As shown in Figure S12D, no ECL response was observed in the control experiment of LPS/chitosan/Fe-MOGs/luminol/GCE without HeLa cells (curve a), eliminating the interference of LPS itself to ECL response. The oxidative stress induced by LPS can be confirmed by comparing the ECL response of HeLa cells with (curve c) and without (curve b) LPS treatment, indicating that induced ROS radicals (excluding H_2O_2) affected little on ECL, which is consistent with the reported literature (Jiang et al. 2018b). On the other hand, when catalase (a selective scavenger of H_2O_2) was added (curve e), the ECL response caused by LPS-treated HeLa cells/chitosan/Fe-MOGs/luminol/GCE (curve d) decreased significantly, referring to the method from literature (Guo et al. 2010). It can be concluded that ECL response is mainly ascribed to the Fe-MOGs-catalyzed H_2O_2 , which is released from HeLa cells through LPS stimulation. Eventually, ECL responses of the as-fabricated biosensor to

various concentrations of HeLa cells were recorded, as illustrated in Figure 3F Inset. The ECL peak intensity is proportional to the number of HeLa cells in a range of 4000 to 300000. The resulting calibration curve is illustrated in Figure 3F and can be represented as $I \text{ (a.u.)} = 1012.2 + 0.0555 n \text{ (} 10^4 \text{)}$ with a square of correlation coefficient of 0.994. The limit of detection (LOD) was estimated to be 42 cells (signal-to-noise ratio of 3). According to the calibration equations obtained from the constructed ECL biosensor, and knowing the cell density, the electrode surface area, the concentration of released H_2O_2 , and volume of electrolyte (4 mL), the amount of H_2O_2 released from HeLa cells under the cell density of $2 \times 10^5 / (\pi \times 0.25 \times 0.25) \text{ cells cm}^{-2}$ was calculated to be around $1 \times 10^{-7} \text{ mol}$. The average number of extracellular H_2O_2 molecules released from per cell (N_0) was calculated according to the Avogadro equation ($n = N_0/N_A$, $N_A = 6.02 \times 10^{23} \text{ mol}^{-1}$) (Guo et al. 2010), which agreed with other reported methods, as shown in Table S1. Therefore, the analysis result can be used as an accurate representation of H_2O_2 production under oxidative stress.

[Figure 3]

[Table 1]

4. Conclusions

In summary, we present an efficient enzyme mimetic with excellent peroxidase-like activity derived from the inspiration of natural enzyme HRP. The Fe-MOGs possesses similar catalytic activity and planar Fe- N_x active sites to HRP. We confirmed that the

high catalytic activity of the Fe-MOGs is attributed to the coordinative Fe-N_x active sites. In a proof-of-concept biosensor, Fe-MOGs significantly promoted the level of sensitivity by amplifying the ECL intensity. Additionally, a possible amplification mechanism of ECL was revealed. Compared with traditional methods for the detection in solution, adhesion of cells on the electrode provided a direct avenue for *in situ* detection of Hela cells with superior sensitivity. We believe this work will help expand understanding of the fundamental mechanism of mimic enzymes by creatively combining activities with the structural information of natural enzymes and further advance the development of different enzyme mimetics in the biosensing field.

Notes

The authors declare no competing financial interest.

Acknowledgements

This research was supported by the National Natural Science Foundation of China (Grant Nos. 21675086 and 62001224), the Natural Science Foundation of Jiangsu Province (No. BK20190457), the Fundamental Research Funds for the Central Universities (Nos. 30918012202 and 30919011213), “Overseas Academic Partnership Program” of Nanjing University of Technology (2019), and a project founded by the priority academic program development of Jiangsu Higher Education Institutions (PAPD). The authors wish also to acknowledge the support from the Sino-French international research network “New nanostructured materials and biomaterials for

renewable electrical energy sources” for providing facilities.

Table 1. Different Methods for H₂O₂ Detection

Electrode material	Method	Linearity (μ M)	LOD (nM)	Advantages	Disadvantages	ref
Cu-MOF/SPE	EC	10-1000, 1400-6800	4100	High flexibility	Time-consuming fabrication	(Ling et al. 2019)
PAN-PNMThH HRP	EC	5-60000	3200	Easy operation	Temperature and pH sensitive	(Chen et al. 2016)
PEP-Npb ₁ -Cy ₃	FL	0-40	260	High specificity	Complex fabrication	(Zhao et al. 2018)
Fe/N-C	ECL	0.001-0.3	0.93	High sensitivity Fast electron transfer	Dynamic range limited Time-consuming fabrication	(Tian et al. 2019)
L012@PAni-PAAm	ECL	0.01-50	2.9	High sensitivity	Complex fabrication	(Xiaojin et al. 2020)
ABEI-Ag@PAni-ATMP	ECL	0.01-200	9.6	Excellent conductivity	Interference	(Xu et al. 2019)
PMT array chip	ECL	1-1000	170	Visualized detection	Software dependent	(Qi et al. 2016)
ABEI-Ag@PAni-PA	ECL	0.01-40	3.3	Good biocompatibility	Complex fabrication	(Jiang et al. 2018b)
Fe-MOGs/luminol	ECL	0.01-40	2.2	High sensitivity	Complex fabrication	This work

References

- Bete, S.C., Wurtele, C., Otte, M., 2019. *Chem. Commun.* 55(30), 4427-4430.
- Chen, C., Hong, X., Xu, T., Chen, A., Lu, L., Gao, Y., 2016. *Synthetic. Met.* 212, 123-130.
- Chen, W.H., Vazquez-Gonzalez, M., Kozell, A., Cecconello, A., Willner, I., 2018. *Small.* 14(5), 1703149.
- Ding, H., Cai, Y., Gao, L., Liang, M., Miao, B., Wu, H., Liu, Y., Xie, N., Tang, A., Fan, K., Yan, X., Nie, G., 2019. *Nano Lett.* 19(1), 203-209.
- Fruehauf, J.P., Meyskens, F.L., Jr., 2007. *Clin. Cancer. Res.* 13(3), 789-794.
- Guo, C.X., Zheng, X.T., Lu, Z.S., Lou, X.W., Li, C.M., 2010. *Adv. Mater.* 22(45), 5164-5167.
- Harrigan, J.A., Jacq, X., Martin, N.M., Jackson, S.P., 2018. *Nat. Rev. Drug. Discov.* 17(1), 57-78.
- He, L., Peng, Z.W., Jiang, Z.W., Tang, X.Q., Huang, C.Z., Li, Y.F., 2017. *ACS Appl. Mater. Interfaces* 9(37), 31834-31840.
- Hou, C.-C., Zou, L., Sun, L., Zhang, K., Liu, Z., Li, Y., Li, C., Zou, R., Yu, J., Xu, Q., 2020. *Angew. Chem. Int. Ed. Engl.* 59(19), 7384-7389.
- Hu, Y., Cheng, H., Zhao, X., Wu, J., Muhammad, F., Lin, S., He, J., Zhou, L., Zhang, C., Deng, Y., Wang, P., Zhou, Z., Nie, S., Wei, H., 2017. *ACS Nano.* 11(6), 5558-5566.
- Jiang, B., Duan, D., Gao, L., Zhou, M., Fan, K., Tang, Y., Xi, J., Bi, Y., Tong, Z., Gao, G.F., Xie, N., Tang, A., Nie, G., Liang, M., Yan, X., 2018a. *Nat. Protoc.* 13(7),

1506-1520.

- Jiang, X., Wang, H., Yuan, R., Chai, Y., 2018b. *Anal. Chem.* 90(14), 8462-8469.
- Jiao, L., Wu, J., Zhong, H., Zhang, Y., Xu, W., Wu, Y., Chen, Y., Yan, H., Zhang, Q., Gu, W., Gu, L., Beckman, S.P., Huang, L., Zhu, C., 2020. *ACS Catal.* 10(11), 6422-6429.
- Kluecker, M., Nawaz Tahir, M., Ragg, R., Korschelt, K., Simon, P., Gorelik, T.E., Barton, B., Shylin, S.I., Panthöfer, M., Herzberger, J., Frey, H., Ksenofontov, V., Möller, A., Kolb, U., Grin, J., Tremel, W., 2017. *Chem. Mater.* 29(3), 1134-1146.
- Lian, M., Chen, X., Lu, Y., Yang, W., 2016. *ACS Appl. Mater. Interfaces* 8(38), 25036-25042.
- Ling, W., Hao, Y., Wang, H., Xu, H., Huang, X., 2019. *Nanotechnology* 30(42), 424002.
- Liu, G., Ma, C., Jin, B.K., Chen, Z., Zhu, J.J., 2018. *Anal. Chem.* 90(7), 4801-4806.
- Liu, Y., Zhou, M., Cao, W., Wang, X., Wang, Q., Li, S., Wei, H., 2019. *Anal. Chem.* 91(13), 8170-8175.
- Lou, Y., Liu, J., Liu, M., Wang, F., 2020. *ACS Catal.* 10(4), 2443-2451.
- Miao, Y.-L., Li, S.-D., Liu, J.-L., Guo, F.-S., Tong, M.-L., 2015. *Inorg. Chem. Commun.* 52, 77-79.
- Mirzaei, M., Eshtiagh-Hosseini, H., Hassanpoor, A., 2019. *Inorg. Chim. Acta.* 484, 332-337.
- Piazza, I., Kochanowski, K., Cappelletti, V., Fuhrer, T., Noor, E., Sauer, U., Picotti, P., 2018. *Cell* 172(1-2), 358-372.
- Qi, L., Xia, Y., Qi, W., Gao, W., Wu, F., Xu, G., 2016. *Anal. Chem.* 88(2), 1123-1127.

- Ramezanpour, B., Mirzaei, M., Jodaian, V., Shahrak, M.N., Frontera, A., Molins, E., 2019. *Inorg. Chim. Acta.* 484, 264-275.
- Shamsipur, M., Molaabasi, F., Sarparast, M., Roshani, E., Vaezi, Z., Alipour, M., Molaei, K., Naderi-Manesh, H., Hosseinkhani, S., 2018. *ACS Sustain. Chem. Eng.*, 11123-11137.
- Singh, N., Savanur, M.A., Srivastava, S., D'Silva, P., Mugesh, G., 2017. *Angew. Chem. Int. Ed. Engl.* 56(45), 14267-14271.
- Sun, X., Guo, S., Chung, C.S., Zhu, W., Sun, S., 2013. *Adv. Mater.* 25(1), 132-136.
- Sun, Y., Silvioli, L., Sahraie, N.R., Ju, W., Li, J., Zitolo, A., Li, S., Bagger, A., Arnarson, L., Wang, X., Moeller, T., Bernsmeier, D., Rossmeis, J., Jaouen, F., Strasser, P., 2019. *J. Am. Chem. Soc.* 141(31), 12372-12381.
- Tian, H., Tan, B., Dang, X., Zhao, H., 2019. *J. Electrochem. Soc.* 166(15), B1594-B1601.
- Wang, J., Huang, R., Qi, W., Su, R., Binks, B.P., He, Z., 2019a. *Appl. Catal. B: Environ.* 254, 452-462.
- Wang, S., Zhao, Y., Wang, M., Li, H., Saqib, M., Ge, C., Zhang, X., Jin, Y., 2019b. *Anal. Chem.* 91(4), 3048-3054.
- Wei, H., Wang, E., 2013. *Chem. Soc. Rev.* 42(14), 6060-6093.
- Wu, J., Wang, X., Wang, Q., Lou, Z., Li, S., Zhu, Y., Qin, L., Wei, H., 2019. *Chem. Soc. Rev.* 48(4), 1004-1076.
- Guo, X.J., Li, Y.B., Li, Y.C., Ye, Z.Y., Zhang, J.J., Zhu, T., Li, F., 2020. *Electrochim. Acta.* 354, 136763.

Xu, L.H., Li, J.J., Zeng, H.B., Zhang, X.J., Cosnier, S., Marks, R.S., Shan, D., 2019.

Biosens. Bioelectron. 143, 111601.

Zhang, Z.Y., 2017. Acc. Chem. Res. 50(1), 122-129.

Zhao, P., Wang, K., Zhu, X., Zhou, Y., Wu, J., 2018. Dyes. Pigments. 155, 143-149.

Figure Captions

Figure 1 (A) UV-vis absorption spectra of (a) PDA, (b) Fe(Ac)₂, (c) Fe-MOGs, (d) Fe-MOGs/luminol, (e) luminol. (B) FT-IR spectra of (a) Fe-MOGs, (b) PDA, (c) Fe(Ac)₂. (C) PL spectra of (a) Fe-MOGs, (b) PDA. (D) SEM image of the unfreeze-dried Fe-MOGs. (E) SEM and (F) TEM images of the Fe-MOGs. (G) The high-resolution XPS survey scans of Fe-MOGs Fe 2p (satellite peaks omitted), (H) N 1s and (I) C 1s.

Figure 2 (A) CVs of bare GCE (a), PDA/GCE (b), Fe-MOGs/GCE (e) in 0.01 M, pH 7.4 PBS, and CVs of bare GCE (c), PDA/GCE (d), Fe-MOGs/GCE (f) in 0.01 M, pH 7.4 PBS containing 1mM H₂O₂, scan rate: 10 mV s⁻¹. (B) CVs of Fe-MOGs modified GCE in 0.01 M, pH 7.4 PBS containing (a) 0, (b) 0.5, (c) 1.0, (d) 1.5 mM H₂O₂, scan rate: 10 mV s⁻¹.

Figure 3 (A) ECL-time responses of (a) Fe-MOGs/luminol/GCE, (b) PDA/luminol/GCE, (c) luminol/GCE and (d) Fe-MOGs/GCE in 0.01 M, pH 7.4 PBS containing 15 μM H₂O₂. Scan rate: 30 mV s⁻¹. (B) ECL-potential curves of (a) Fe-MOGs/luminol/GCE and (b) luminol/GCE in 0.01 M, pH 7.4 PBS containing 15 μM H₂O₂. Scan rate: 30 mV s⁻¹. **Inset B:** CVs of (a), (b) in 0.01 M, pH 7.4 PBS containing 15 μM H₂O₂, scan rate: 10 mV s⁻¹. (C) The calibration plot of ECL peak intensity versus H₂O₂ concentration from 0.01 to 40 μM. Error bars, SD, n = 3. **Inset C:** ECL-time response of the Fe-MOGs/luminol/GCE at different concentrations of H₂O₂ in 0.01 M, pH 7.4 PBS during a continuous potential scan between 0 and 0.8 V. Scan rate: 30 mV s⁻¹. (D) The calibration plot of ECL peak intensity versus H₂O₂ concentration from 0.01 to 1 μM. Error bars, SD, n = 3. (E) The calibration plot of ECL peak intensity versus

H₂O₂ concentration from 1 to 40 μM. Error bars, SD, n = 3. **(F)** The calibration plot of ECL peak intensity versus Hela cells number from 4,000 to 300,000. **Inset F:** ECL-time response of the Fe-MOGs/luminol/GCE toward different concentrations of Hela cells in 0.01 M, pH 7.4 PBS during a continuous potential scan between 0 and 0.8 V. Scan rate: 10 mV s⁻¹.

Scheme 1 Schematic illustration of the fabrication process of the Fe-MOGs/luminol ECL biosensor for Hela cells.

Figure 1

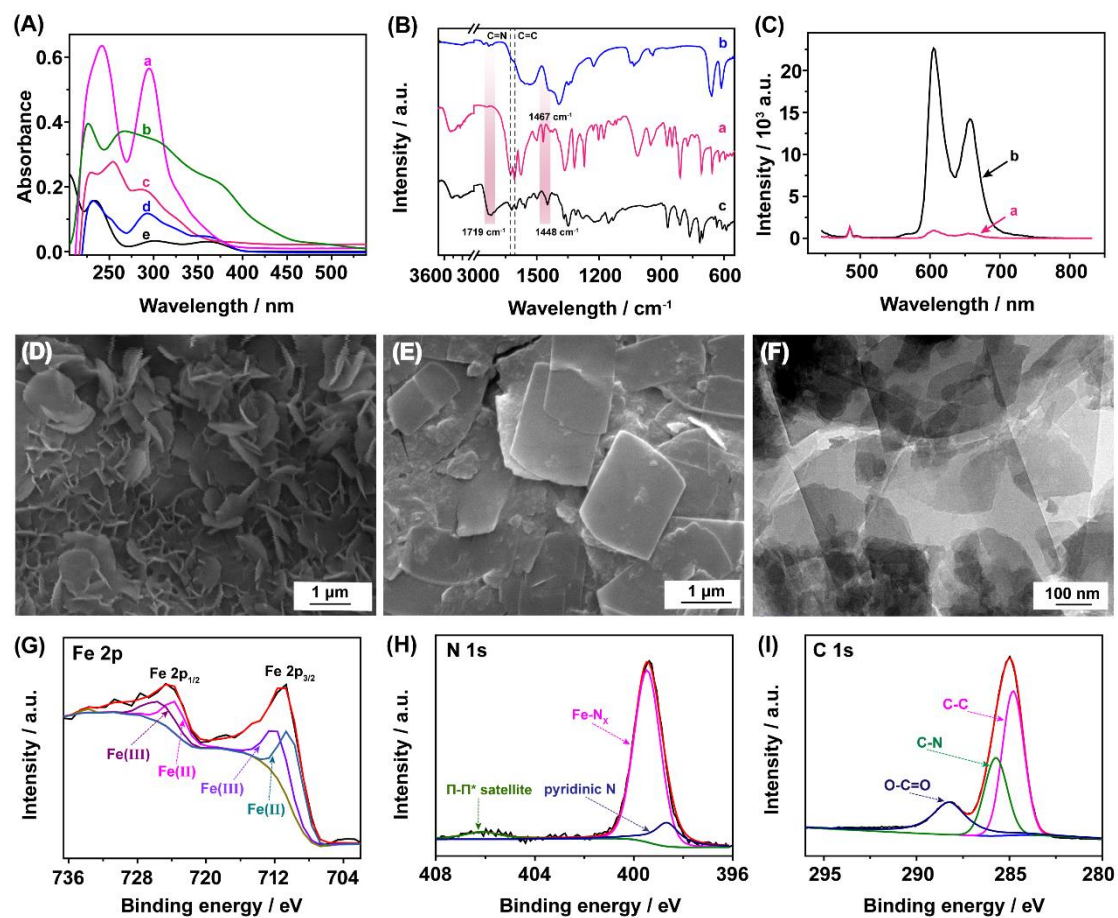


Figure 2

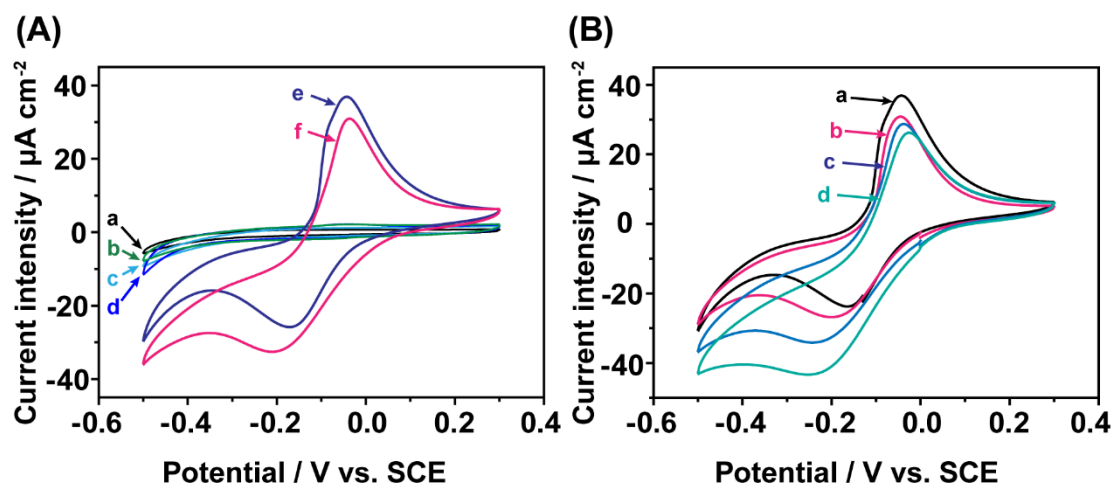
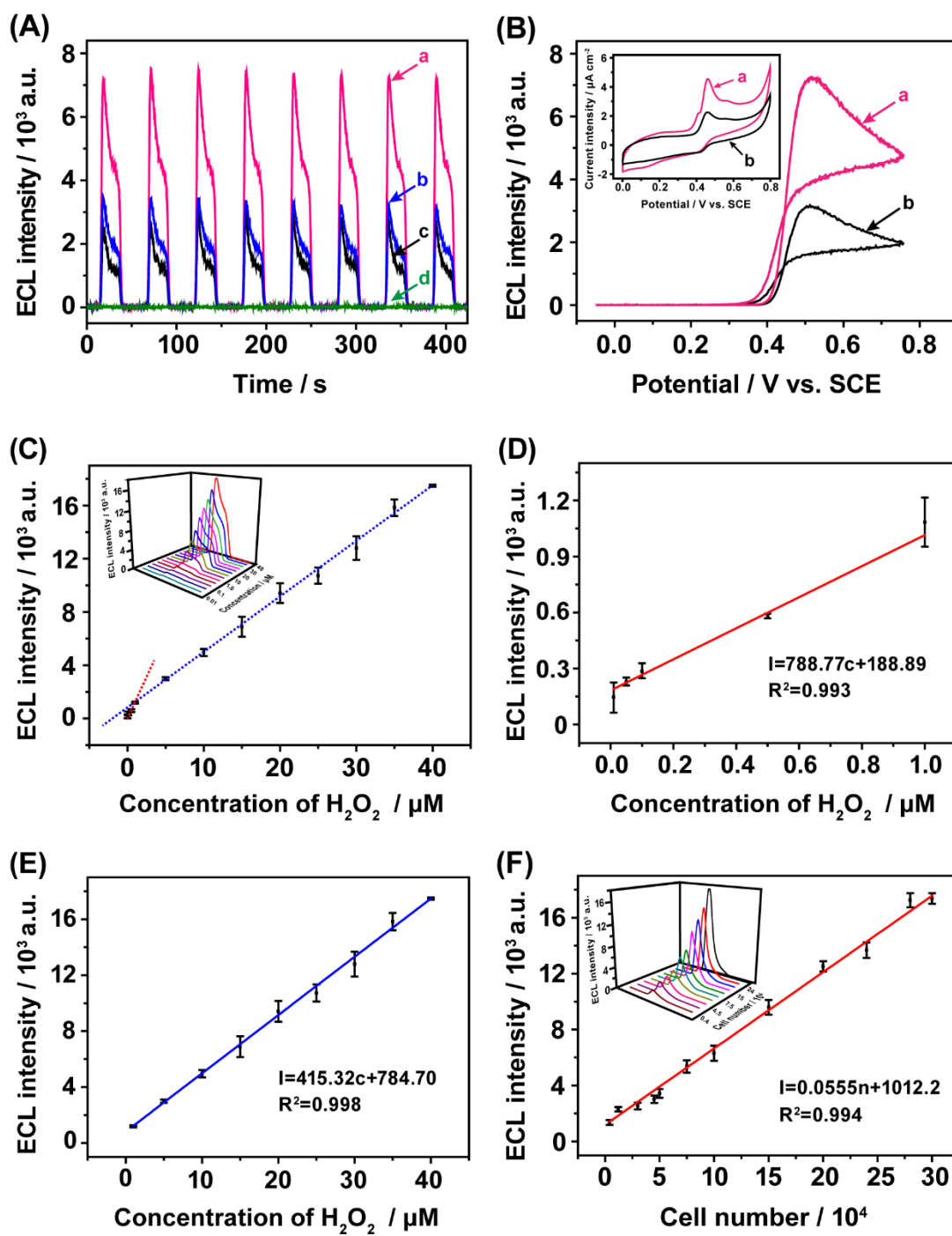
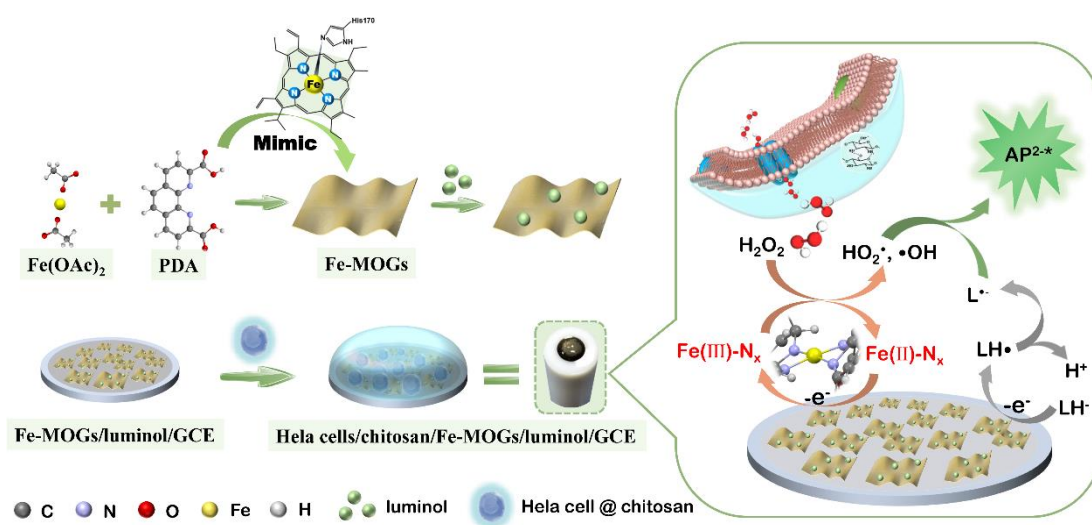


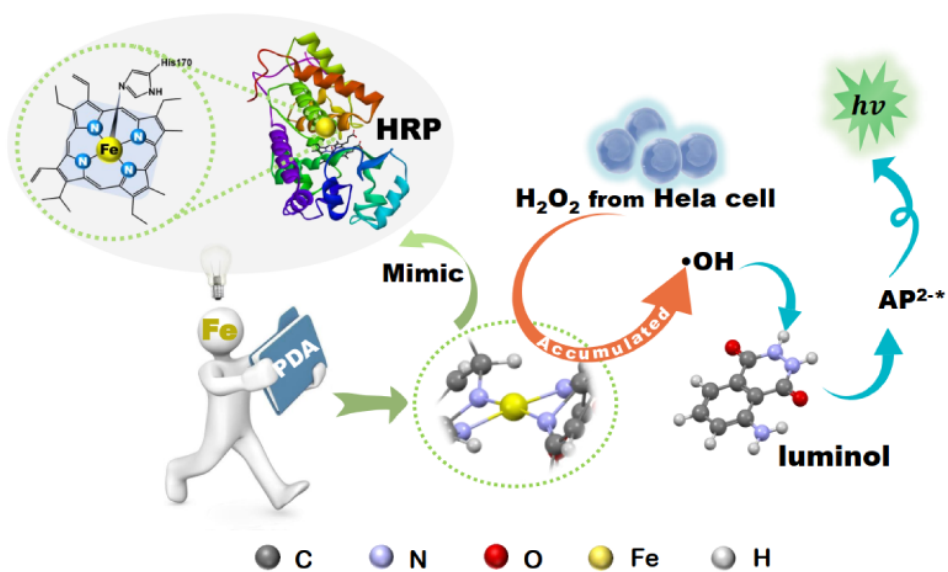
Figure 3



Scheme 1



TOC



For Table of Contents Only

